EXTRACTION OF SEA ICE AREA USING AVHRR DATA OF NOAA SATELLITE

Shinya TANAKA,

Space Systems Development Department, Fujitsu Ltd.,
17–25, Shinkamata 1-chome, Ota-ku, Tokyo 144

Takashi YAMANOUCHI and Sadao KAWAGUCHI

National Institute of Polar Research, 9–10, Kaga 1-chome, Itabashi-ku, Tokyo 173

Abstract: This paper presents a new method for extracting sea-ice information from the multi-spectral AVHRR images (visible, near-infrared and infrared images) of a TIROS-N/NOAA series satellite.

The original image data are calibrated and corrected. The difference in albedo (reflectivity) between visible and near infrared images is obtained. Further, the difference in the brightness temperature between the 3.7 and 11 μm infrared images is computed. The resulting images are formed from these two difference images and displayed on the image display using the false color technique. By applying this method to data observed during the daytime, the sea ice area and cloud area can be easily distinguished.

1. Introduction

A NOAA series meteorological satellite, which orbits the earth every 102 min at an average altitude of 854 km, observes the earth's surface along its flight path and constantly transmits data by High Resolution Picture Transmission (HRPT). HRPT consists mainly of Advanced Very High Resolution Radiometer (AVHRR) data. These AVHRR images provide valuable information about weather conditions. Several methods have been proposed for the discrimination of cloud area from satellite data (PHULPIN *et al.*, 1983; AOKI, 1982). However, on snow cover and sea ice, it is often difficult to distinguish clouds from ice using the satellite's raw image data because the difference of temperature between the clouds and sea ice is very small and the difference of albedo between the clouds and ice is also very small in the visible region. For these reasons, it has been necessary to develop a method for extracting sea ice.

This paper presents a method for separating sea ice from clouds using image data of the Antarctic zone obtained from the meteorological satellite.

2. Data

The earth emits electromagnetic waves toward space mainly in the infrared region. The sun emits in the visible region. These emissions correspond to black body emissions of about 280 K (earth) and 6000 K (sun). The AVHRR instrument

sensors can detect emissions from the earth and the reflected solar radiation. AVHRR is a five-channel instrument. Table 1 shows the spectral characteristics of the AVHRR instrument.

The data analyzed in this paper are HRPT data received at Syowa Station by the 22nd and 23rd Japanese Antarctic Research Expeditions.

Figure 1 shows the pre-processing flow chart. The first step is the extraction of AVHRR data from the HRPT data. The second step is calibration (LAURITSSON et al., 1979). In this step, the raw visible and near infrared images are converted into albedo, and infrared images are converted into brightness temperature. The third step is projection on a polar stereo map and extraction of the region to be analyzed. The region used in this analysis is about 500×500 km area around the Lützow-Holm Bay including Syowa Station as shown in Fig. 2.

The results of the pre-processing from the image taken by NOAA-7 on Rev. 2937 at 1350 (GMT) on January 17, 1982, are shown in Figs. 3, 4 and 5. Figure 3 shows
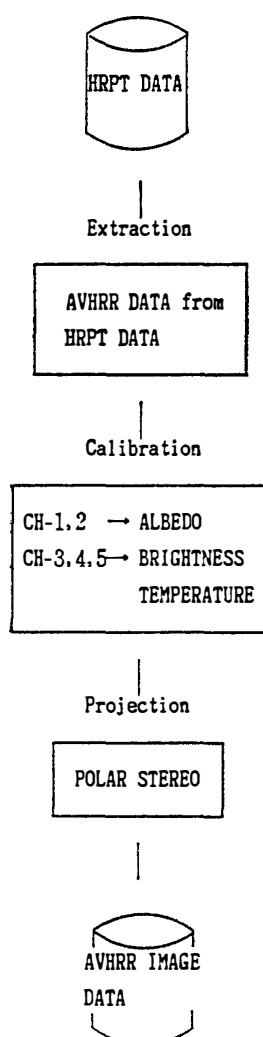
Table 1. Spectral characteristics of the NOAA-7 AVHRR.

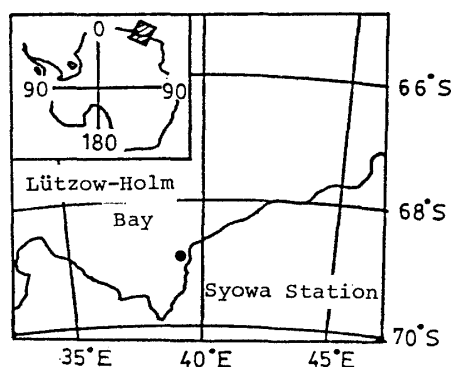| Channel No.	Spectral region	Remarks
CH-1	0. 58 – 0. 68 μm	Visible
CH-2	0. 725– 1. 1 μm	Near infrared
CH-3	3. 55 – 3. 93 μm	Infrared
CH-4	10. 3 –11. 3 μm	Infrared
CH-5	11. 5 –12. 5 μm	Infrared

Fig. 1. Pre-processing flow chart of AVHRR data.

Fig. 2. Region map of analyzed area in Antarctica.
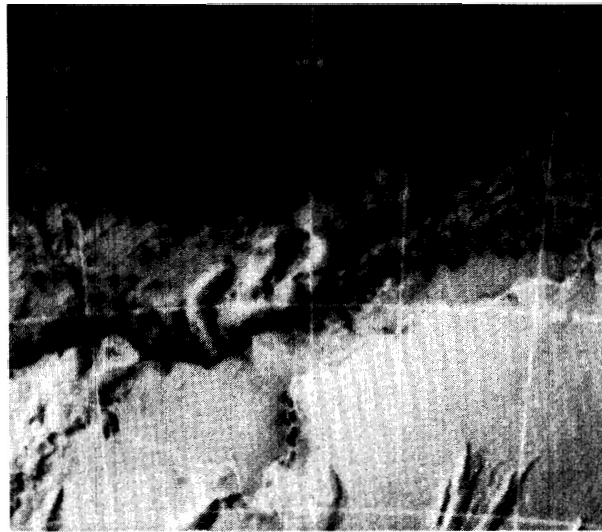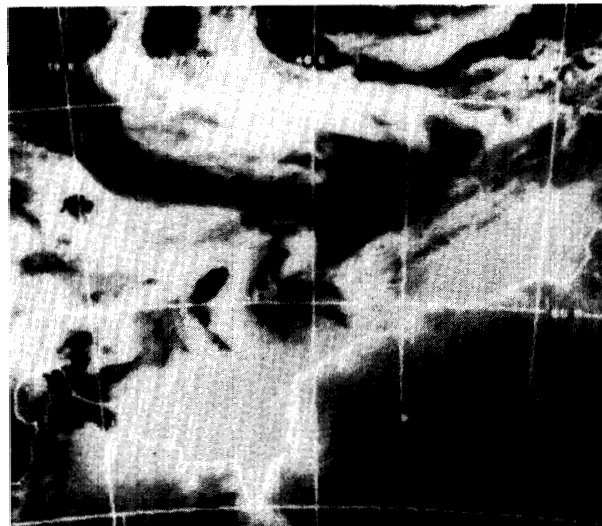
Figs. 3–5.   Images of NOAA-7 AVHRR 1350 GMT, January 17, 1982.
             Albedo image of CH-1 (Fig. 3), brightness temperature images
             of CH-4 (Fig. 4) and CH-5 (Fig. 5).

the visible image (CH-1) converted into albedo and which contains clouds, sea ice and seawater. As can be seen, it is very difficult to distinguish between clouds and sea ice. Figure 4 shows the CH-4 infrared image converted into brightness temperature. In this picture, clouds, sea ice and seawater are also very hard to distinguish. Finally, Fig. 5 shows the CH-3 brightness temperature image which includes the earth's emission and reflected solar radiation.

3. Extraction of Cloud and Sea Ice

This section describes the method for extracting clouds and sea ice using the AVHRR data obtained during the daytime in the Antarctic zone.

3.1. Cloud extraction

The area covered by clouds is extracted by using both the CH-3 and CH-4 images. The CH-4 sensor detects the energy of the wavelength in the range of 10.3 to 11.3 μm. In this region, the influence of solar radiation is negligible so that only the thermal radiation from the earth's surface and clouds is detected by the sensor.

The CH-3 sensor detects energy in the wavelength range 3.5 to 4.0 μm. In this wavelength region emissions from both the surface and clouds and solar radiation reflected by the clouds are detected by the sensor. Because of the high reflectivity of clouds, the brightness temperature of the cloud region seems to be much higher than that of other areas (MELLOR, 1977; WARREN, 1982; WISCOMBE and WARREN, 1980; YAMAMOTO et al., 1970). This can be seen in Fig. 5, where the bright area corresponds to clouds. Reflectivity of 3.7 μm radiance by clouds was already discussed by BELL and WONG (1981) using AVHRR data. RASCHKE and REICHENAUER (1983) also proposed to use these two channels to extract the cloud region over the Antarctic
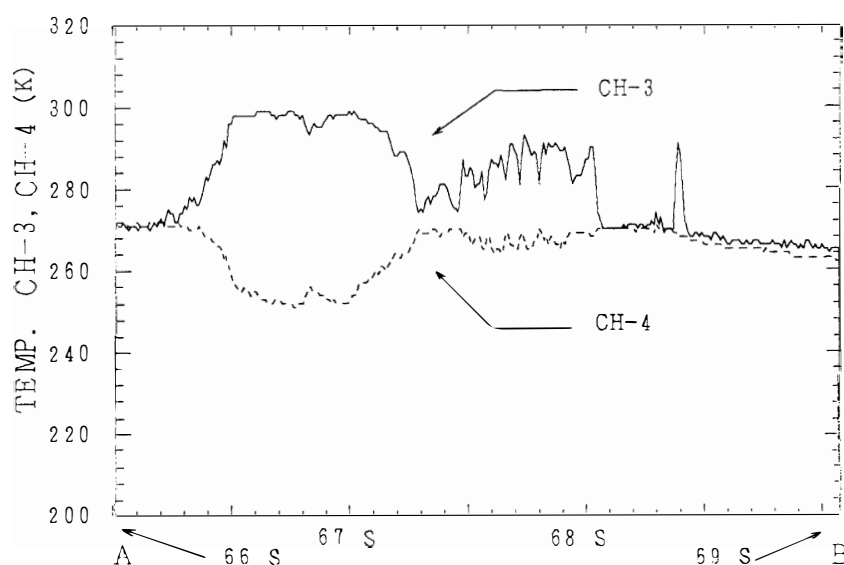

Fig. 6. Brightness temperature of CH-3 and CH-4 of NOAA-7 AVHRR on January 17, 1982 along the meridian of 42°E from 66 to 69°S.

snow cover.   They considered theoretically the difference in the emissivity and albedo between the cloud and snow.

Figure 6 shows the brightness temperature graph of CH-3 and CH-4 taken along the 42.0°E longitude extending from 66.0 to 69.0°S (see Figs. 4 and 5).   The graph for CH-3 shows that the brightness temperature of the cloud area is higher than that of the other areas.   Assuming that CH-4 shows surface temperature, subtracting CH-4 from CH-3 ignoring atmospheric absorption leaves only the reflection of solar radiation.

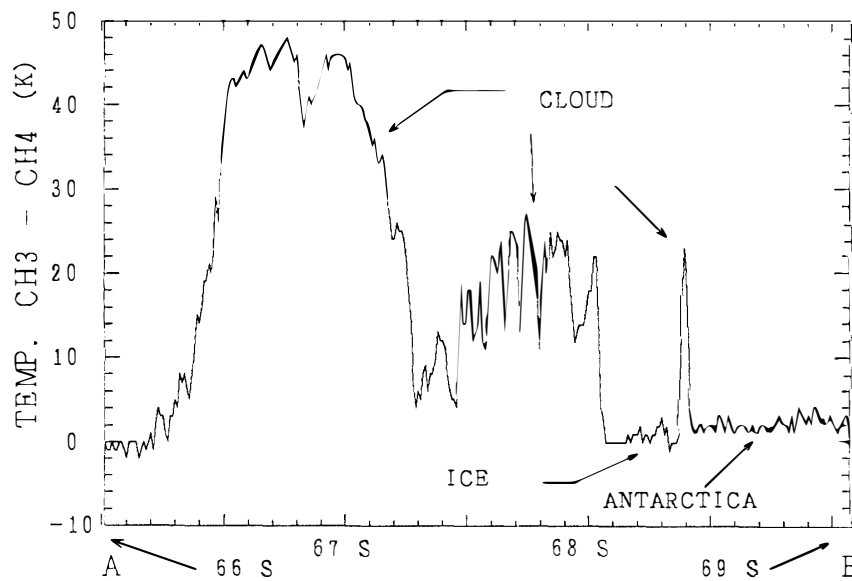Figure 7 shows the graph taken along the line from the image obtained by

Fig. 7.   *Difference of brightness temperature between CH-3 and CH-4 of NOAA-7 AVHRR on January 17, 1982 along the meridian of 42°E from 66 to 69°S.*

Fig. 8.   *Pseudo color image obtained by subtracting the brightness temperature of CH-4 from CH-3.   NOAA-7 AVHRR on January 17, 1982.*

subtracting the brightness temperature of CH-4 from that of CH-3. The figure shows that areas with a large difference of brigtness temperature correspond to areas where clouds are present.

Figure 8 shows the pseudo color image obtained by subtracting the brigtness temperature of CH-4 from CH-3 (over 0%: blue, below 0%: red). The blue region corresponds to clouds, and the red region corresponds to areas other than clouds. It is obvious that cloud, rock and other areas can be distinguished.

3.2. Sea ice extraction

After extracting clouds, the area covered by ice and snow is extracted by using the CH-1 and CH-2 images.

The CH-1 sensor detects energy in the wavelength range 0.58 to 0.68 μm. In this region, it detects only the solar radiation reflected by the earth's surface and clouds.

The CH-2 sensor detects energy in the wavelength range 0.725 to 1.1 μm and also detects reflected solar radiation. However, the albedo of CH-1 and CH-2, which depends on the surface conditions, is different (MELLOR, 1977; WARREN, 1982; WISCOMBE and WARREN, 1980; DAGGIN et al., 1982). In the near infrared region, different from the visible region, the albedo of snow is sensitive to grain size and is different from the albedo of ice (WARREN, 1982; DOZIER, 1981).

Figure 9 shows the albedo graph of CH-1 and CH-2 taken along the line of Fig. 3. The absolute value of the albedo in the figure is arbitrary, since the correction of the incident solar flux depending on solar zenith angle and the inflight calibration have not been made. Albedos of CH-1 and CH-2 are different. It is assumed that the difference in albedo is a function of the surface condition (open sea, ice or clouds). Figure 10 shows the result of subtracting the albedo of CH-2 from CH-1. It is clear that the difference in albedo is small in the area of open sea, but that in the ice, snow
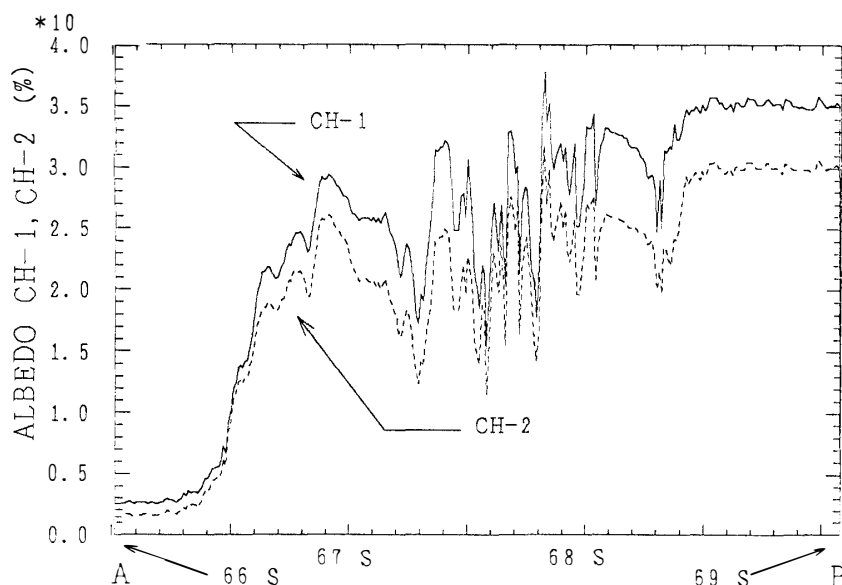

Fig. 9. Albedo of CH-1 and CH-2 of NOAA-7 AVHRR on January 17, 1982 along the meridian of 42°E from 66 to 69°S.

and cloud area, the difference in albedo is large.   It is assumed that the difference in albedo in the snow area (Antarctic continent) is smaller than that in the ice area.

Figure 11 shows the pseudo color image resulting from subtracting the albedo of CH-2 from CH-1 (0–2%: red, 2–5%: green, 5%–: blue).   Although the cloud area cannot be extracted from the image, it can be assumed that the red area shows the sea, rocks and cloud areas, the green area shows sea ice and clouds, and the blue area shows snow and clouds.
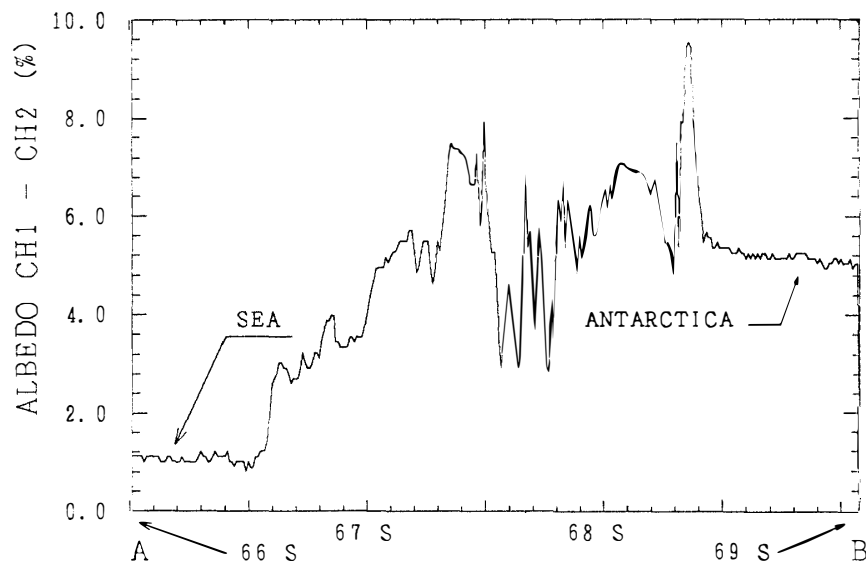

Fig. 10.   Difference of albedo of CH-1 and CH-2 of NOAA-7 AVHRR on January 17, 1982 along the meridian of 42° E from 66 to 69° S.
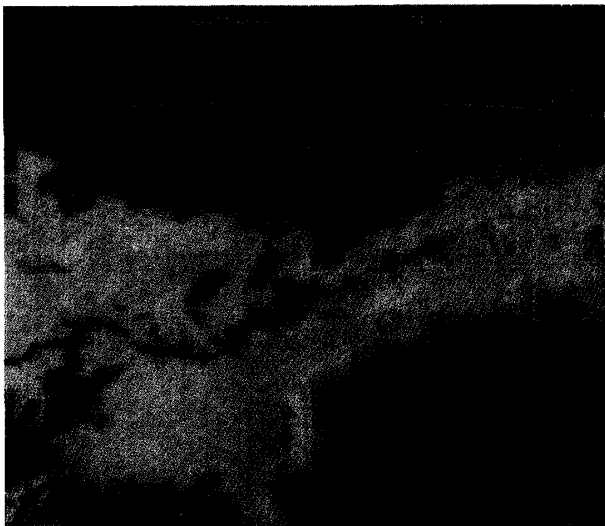

Fig. 11.   Pseudo color image obtained by subtracting the albedo of CH-2 from CH-1. NOAA-7 AVHRR on January 17, 1982.
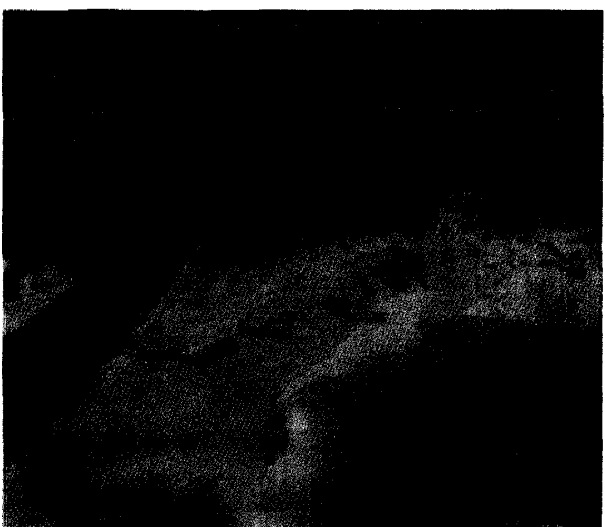
Fig. 12. False color images obtained by synthesizing three color images. Green: difference of albedo of CH-1 and CH-2, blue: difference of brightness temperature of CH-3 and CH-4, red: brightness temperature of CH-4.

a. NOAA-7 AVHRR, 1410 GMT, December 29, 1981.

b. NOAA-7 AVHRR, 1350 GMT, January 17, 1982.

c. NOAA-7 AVHRR, 1335 GMT, February 13, 1982.

4. False Color Technique

The previous section described a method in which multispectral analysis is used to extract clouds and sea ice by synthesizing two analyzed images so that the areas can be easily distinguished.

Figure 12 shows the images created using the false color image technique of synthesizing three channels (green, blue and red channels). The image for the green channel is the result of subtracting the albedo of CH-2 from CH-1, based on the assumption that the difference in albedo indicates the surface condition. The image for the blue channel is the result of subtracting the brightness temperature of CH-4 from CH-3. It is assumed that the large difference in the brightness temperature indicates a cloud and rock region. The image for the red channel is the brightness temperature of CH-4. It can be assumed that CH-4 shows the surface or cloud-top temperature (ignoring atmospheric absorption).

From these false color images, sea ice can be distinguished from the sea and clouds. The red area shows the open sea (including shadow from clouds and rocks). The green area shows the snow, the yellow area sea ice and continental ice, and the blue area clouds. The boundary between ice and snow is still arbitrary. In the area covered with thin clouds, the sea ice edge can be detected by the difference in color between blue-green and dark blue, for sea ice and open sea, respectively.

5. Conclusion

It is difficult to distinguish the ice and clouds using only the brightness temperature or albedo. The false color method in this paper has great promise for detecting sea ice edges under clouds. This kind of technique is indispensable for the study of sea ice and cloud climatology in the polar regions. This technique is also very useful in the practical sense for scientific expeditions and ship voyages in the Antarctic to obtain sea ice and cloud information immediately. However, the determination of the threshold level for detecting ice and clouds is still uncertain, because the radiation properties of the ice, colud and sea surface in the 3.7 μm region are not known in detail. More studies of these radiation properties are needed.

References

AOKI, T. (1982): An improved method to retrieve the clear column radiance from partically cloudy spots of radiometer on board satellite. J. Meteorol. Soc. Jpn., **60**, 758–764.

BELL, G. J. and WONG, M. C. (1981): The near-infrared radiation received by satellites from clouds. Mon. Weather Rev., **109**, 2158–2163.

DAGGIN, M. J., SCHOCK, L. and GRAY, T. I. (1982): Effect of sub-pixel sized cloud on vegetation assessment from satellite data. Adv. Multispect. Remote Sensing Technol. Appl., SPIE, **345**, 94–101.

DOZIER, J. (1981): Effect of grain size and snowpack water equivalence on visible and near-infrared satellite observation of snow. Water Resour. Res., **17**, 1213–1221.

LAURITSSON, L., NEISON, G. J. and PORTO, F. W. (1979): Data extraction and calibration of TIROS-N/NOAA radiometers. NOAA Tech. Memo., NESS, **107**, 58 p.

MELLOR, M. (1977): Engineering properties of snow. J. Glaciol., **19**, 50–66.

PHULPIN, T., DERRIEN, M. and BRARD, A. (1983): A two-dimensional histogram procedure to

analyze cloud cover from NOAA satellite high-resolution imagery. J. Climate Appl. Meteorol., **22**, 1332–1345.

RASCHKE, E. and REICHENAUER, H. (1983): Satellite observations of clouds and haze over the Antarctic continent. Paper presented at the Symposium on Polar Meteorology and Climatology (PM-1) at IUGG Hamburg, 421.

WARREN, S. G. (1982): Optical properties of snow. Rev. Geophys. Space Phys., **20**, 67–89.

WISCOMBE, W. J. and WARREN, S. G. (1980): A model for the spectral albedo of snow. I; Pure snow. J. Atmos. Sci., **37**, 2712–2733.

YAMAMOTO, G., Tanaka, M. and ASANO, S. (1970): Radiative transfer in water clouds in the infrared region. J. Atmos. Sci., **27**, 282–292.